N-fused porphyrin with pyridinium side-arms : A new class of aromatic ligand with DNA-binding ability

Ikawa, Yoshiya
International Research Center for Molecular Systems, Kyushu University | Department of Chemistry and Biochemistry, Graduate School of Engineering, Kyushu University | Department of Chemistry and Biochemistry, Graduate School of Engineering, Kyushu University

Touden, Satoshi
Department of Chemistry and Biochemistry, Graduate School of Engineering, Kyushu University

Furuta, Hiroyuki
International Research Center for Molecular Systems, Kyushu University | Department of Chemistry and Biochemistry, Graduate School of Engineering, Kyushu University

出版情報：Organic & Biomolecular Chemistry. 9 (23), pp.8068-8078, 2011-12. Royal Society of Chemistry
バージョン：

N-fused porphyrin with pyridinium side-arms: A new class of aromatic ligand with DNA-binding ability

Yoshiya Ikawa,[a,b] Satoshi Touden, [a] and Hiroyuki Furuta*[a,b]

[a]Department of Chemistry and Biochemistry, Graduate School of Engineering, Kyushu University, 744 Moto-oka, Nishi-ku, Fukuoka 819-0395, Japan.

[b]International Research Center for Molecular Systems, Kyushu University, 744 Moto-oka, Nishi-ku, Fukuoka 819-0395, Japan.

Abstract

N-fused porphyrin (NFP) is a porphyrin analogue with an 18π tetrapyrrolic macrocycle in which a unique tripentacyclic ring is embedded. While optical properties of NFP to absorb and emit near-infrared (NIR) light around 1000 nm are promising for its application to NIR technology, its unique structure is also attractive as a platform to construct a novel class of DNA-binding ligands. Herein, we have synthesized a water-soluble derivative of NFP (**pPyNFP**) possessing four cationic pyridinium substituents, and examined its acid/base behaviors and interactions with various forms of DNAs in aqueous solution. **pPyNFP** interacts with ssDNA and dsDNA electrostatically. **pPyNFP** also interacts with a G-quadruplex DNA derived from human telomeric sequence and causes characteristic spectral change of the G-quadruplex DNA, which suggests that **pPyNFP** modulates the Na^+-induced (2+2) antiparallel G-quadruplex to the all-parallel structure.

A table of contents entry

A water-soluble derivative of N-fused porphyrin (NFP) modulates G-quadruplex DNA structure

Introduction

Porphyrins and their related pigments play pivotal roles in living cells.[1] While naturally occuring porphyrins usually form complexes with proteins, structural feature of porphyrin is also attractive as DNA-binding ligands. Actually, porphyrins possessing pyridinium moieties such as 5,10,15,20-tetrakis(4'-*N*-methylpyridyl)porphyrin (**TMPyP**, Chart 1) and 5,10,15,20-tetrakis(α-pyridinio-*p*-tolyl)porphyrin (**pPyP**, Chart 1) constitute a representative class of water-soluble porphyrins with DNA-binding ability.[2-4] In **TMPyP** and **pPyP**, four cationic pyridinium moieties afford not only high water-solubilty but also electrostatic affinity for sugar-phosphate backbones of DNA. A large number of DNA-binding studies of **TMPyP**, **pPyP**, and their derivatives have provided a basic framework of porphyrin-DNA interactions.[2-8] These data are not only improtant for biological and diagnostic applications but also useful for the development of new classes of DNA-binding ligands because a variety of novel platforms for DNA-binding ligands are synthesized along with the development of porphyrin-related maclocycles (porphyrinoids).[9-13] Although DNA-binding ability has been vested to several porphyrinoids recently, the rest of them have still remained unexploited as DNA-binding ligands.[14-20]

N-fused porphyrin (NFP) is a class of porphyrinoids with an 18π tetrapyrrolic macrocycle in which a unique tripentacyclic ring was embedded.[21-25] Regardless of its peculiar structure, NFP can be readily prepared in two steps from a porphyrin isomer, N-confused porphyrin (NCP, Chart 2).[22,23] NFP has been attractive as a near-infrared

(NIR) dye applicable to material science because of its photophysical properties to absorb and emit NIR light around 1000 nm.[26] Crystal structure of N-fused tetraphenylporphyrin (**NFTTP**, see Scheme 1) revealed that the tripentacyclic structure provides a unique π-plane and diminishes the steric hindrance between the aryl moiety at C(5) position and the macrocycle. The dihedral angle between tripentacyclic ring and C(5) phenyl group (25.6°) in **NFTTP** is much smaller than that between ordinary porphyrin plane and *meso*-phenyl group (64.3°).[22] Although these structural features of NFP are attractive as a new class of porphyrin-related DNA-binding ligand, such ability of NFP has been totally unexploited. In this paper, the synthesis of water-soluble **NFTPP** derivative possessing four α-pyridino-*p*-tolyl moieties and its acid/base and DNA-binding properties in aqueous solutions are described.

Results and discussion

Synthesis of NFP derivative with cationic side-arms

To solubilize **NFTPP** in aqueous media, we have designed and synthesized N-fused tetrakis(α-pyridino-*p*-tolyl)porphyrin (**pPyNFP**). The cationic α-pyridino-*p*-tolyl moiety should afford high water-solubility. The target compound (**pPyNFP**) was derived from the N-confused porphyrin (**1**) possessing four methoxymethyl (MOM) ethers (Scheme 1). At first, **1** was synthesized by an acid catalyzed condensation of pyrrole and *p*-methoxymethylbenzaldehyde with methanesulfonic acid (MSA), followed by oxidation with 2,3-dicyano-5,6-dichloro-*p*-benzoquinone (DDQ).[12] Treatment of **1** with *N*-bromosuccinimide (NBS) afforded the dibrominated derivative (**2**), which can be

readily transformed to the N-fused porphyrin derivative (**3**) by treatment with pyridine.[22,23] After removal of the bromo group at C(21) position to yield **4**, the four MOM-ethers in **4** were converted to hydroxy groups to afford **5**. After mesylation of the hydroxy groups in **5** quantitatively, the target compound (**pPyNFP**) was produced by the nucleophilic substitution of mesylate esters in **6** with pyridine. **pPyNFP** was purified by a reverse phase HPLC with CH_3CN/H_2O containing 0.1% trifluoroacetic acid (TFA) and stored as a TFA salt. In DMF, the absorption spectrum of **pPyNFP** was nearly identical to that of **NFTPP** (Fig. 1), indicating that the α-pyridinomethylene moiety did no strongly perturb the electronic state of NFTPP skeleton. Solubility of **pPyNFP** in water was confirmed by partition experiments between ultrapure water and CH_2Cl_2, in which **pPyNFP** was selectively dissolved in water-phase (Fig. S1A).

Acid-base property of PyNFP

Acid-base property of the molecule of interest is often important for its applications in aqueous media and cellular environment. While the acid-base properties of regular porphyrins have been studied extensively,[27-29] those of porphyrin analogues have been scarcely reported.[12,25,30] Previously we studied the acid-base property of a water-soluble NFP derivative (**NFP-R9**, Chart 3) possessing a phenyl substituent at C(21) position, in which the NFP skeleton underwent a two-step protonation to yield mono- and dication in a stepwise manner.[25] The substituent at C(21), however, causes electronic perturbation on the NFP skeleton.[23] Therefore it is desirable to determine the acid-base property of N-fused porphyrin without a C(21) substituent in aqueous solution and, for

such a purpose, the structure of **pPyNFP** is suitable (Scheme 1).

Acid-base property of **pPyNFP** in aqueous solution was investigated under a wide range of pH, adjusted with HCl (acidic region) or NaOH (basic region). Through the pH titration experiments with **pPyNFP**, we observed two pH regions in which the absorption spectra were essentially unchanged (Fig. S1). In the pH region between 8.3 and 11.7, the absorption spectra of **pPyNFP** (Fig. S1B), which were similar to those of **NFTPP** and **pPyNFP** in DMF (Fig. 1), exhibit three Soret-like bands (S-I to S-III) at 359, 494, and 547 nm and Q-like bands at 649, 702, 861, and 949 nm (Fig. S1B). In the pH region between 2.2 and 5.0, the absorption spectra of **pPyNFP** (Fig. S1C) were closely similar to those of the protonated form of **NFTPP** in organic solvent. These observations clearly indicate that **pPyNFP** exists as a freebase (neutral) form at pH 8.3–11.7 and a protonated form (monocation) at pH 2.2–5.0, respectively. With a decrease of pH from 8.3 to 5.0, transition from the freebase to the monocation was clearly observed (Fig. 2A). At the strongly acidic region (pH <2.2), the monocation further decreased the intensity of the Soret-like bands and weakly increased the intensity at the NIR region (Fig. 2B), suggesting that **pPyNFP** monocation accepted the second proton to form a dication. Since a similar two-step spectral change was also reported for **NFP-R9** (Chart 3),[25] the two-step protonation would be an intrinsic property of the NFP skeleton. From the titration curve, the pK_a values of each protonation process, [**2H$^+$-pPyNFP**]//[**H$^+$-pPyNFP**] and [**H$^+$-pPyNFP**]//[**pPyNFP**], were estimated to be 1.3 and 7.0, respectively. These pK_a values were comparable to those for **NFP-R9** (2.3 for [**2H$^+$-NFP-R9**]//[**H$^+$-NFP-R9**], and 6.5 for

[**H**$^{+}$**-NFP-R9**]//[**NFP-R9**]).[25]

Aggregation behavior of pPyNFP

Aggregation properties of **pPyNFP** were examined in a 50 mM HEPES buffer solution because the cationic regular porphyrins including **pPyP** are reported to form several types of aggregates depending on the buffer conditions.[4,31-33] Sodium dodecyl sulfate (SDS), whose critical micellar concentration in H_2O is 8.2 mM, has been shown to modulate the aggregation states of regular porphyrins in aqueous solution.[33] When SDS (5 mM in the final) was added to a buffer solution of **pPyNFP** at pH 8.5, a strong hyperchromic effect was observed without a shift of absorption maxima (λ_{max}) (Fig. 3A). This spectrum change was too large to be attributed to a small pH change (8.5 to 8.35) caused by SDS (see also Fig. S1B). Similar SDS-induced hyperchromic effects were also observed at pH 7.0 (which changed to 6.88 by 5 mM SDS) and pH 5.0 (which changed to 5.12 by 5 mM SDS) albeit hyperchromic effects under neutral and acid conditions were weaker than that under basic conditions (Figs. 3A and 3B). These results indicate that, in 50 mM HEPES buffer solutions, **pPyNFP** should assemble without any particular order because no large shift of λ_{max} characteristic for *H*- or *J*-aggregates was observed (Scheme 2). Regardless of pH in the solution, additions of 1 mM SDS caused hypochromic changes (Fig. 3). Under the 1 mM SDS conditions, **pPyNFP** and SDS presumably form hydrophobic aggregates (Scheme 2), in which the SDS concentration is sufficient to neutralize cationic charges of the pyridinium moieties of **pPyNFP** but too low to disperse **pPyNFP**. **pPyP** also exhibited two-step,

SDS-dependent spectral changes in 50 mM HEPES buffer solutions (Fig. S2).

Interactions with double- and single-stranded DNAs

Recently DNA-binding studies of porphyrin analogues have been reported, and some of them exhibited characteristic properties distinct from regular porphyrins.[9-12] Therefore it is of interest to investigate the interactions between DNA and **pPyNFP** whose pyridinium side-arms should have the ability of electrostatic interactions with the sugar-phosphate backbones of DNA.

We first investigated the interactions to the long double-stranded DNA (dsDNA) in a pH 7.0 buffer solution, in which **pPyNFP** exists as a mixture of freebase and monocation (Fig. 2A). Upon an addition of less than equimolar amount of DNA base pair, **pPyNFP** exhibited a hypochromic change with a red-shift, in which *S-II* was shifted from 485 to 493 nm (Fig. 4A). In the presence of more than one equivalent molar amount of DNA base pair, however, **pPyNFP** exhibited a hyperchromic spectral change without a further shift of λ_{max} (*S-II* was 495 nm) (Fig. 4B).[34] Such two-step changes were not observed in the regular porphyrin (**pPyP**) whose spectral changes induced by dsDNA were unidirectional (a red-shift of the Soret band (414 to 421 nm) with hypochromic change). To investigate whether **pPyNFP** induces the structural change of dsDNA, we measured the circular dichroism (CD) spectra of dsDNA which showed the CD signal of B-form DNA in the range of 220–300 nm (Fig. 4C). Upon addition of **pPyNFP**, the CD signal of dsDNA was diminished (Fig. 4C).

In the presence of less than equimolar amount of dsDNA base pair, dsDNA

may act as a glue or raft, on which **pPyNFP** was condensed (Scheme 2). While this mode of association should accompany hypochromic shift, the observed bathochromic shift (red-shift) should be caused by the interaction between NFP macrocycle and dsDNA. In the presence of excess molar amount of dsDNA base pair, the dense aggregation of **pPyNFP** on dsDNA should be resolved but the interaction between the NFP macrocycle and dsDNA should be retained (Scheme 2).

To see whether A:T and G:C base pairs cause different effects on **pPyNFP**, we examined the effects of two synthetic DNAs (5'-ATATATATATATATATATAT-3': $d(AT)_{10}$) and 5'-GCGCGCGCGCGCGCGCGCGC-3': $d(GC)_{10}$) which can form duplexes with only A:T and G:C base pairs (designated as $[d(AT)_{10}]_2$ and $[d(GC)_{10}]_2$), respectively. Upon additions of these two DNAs, overall patterns of the spectral changes resembled those caused by dsDNA (Fig. 5A and 5B). On the other hand, the hypochromic change and its recovery were more remarkable with $[d(AT)_{10}]_2$ (Fig. 5A) than with $[d(GC)_{10}]_2$ (Fig. 5B). To further investigate the interactions between **pPyNFP** and $[d(AT)_{10}]_2$ and $[d(GC)_{10}]_2$, CD spectra induced in the Soret band of **pPyNFP** were measured (Fig. 5C & 5D). In the presence of 1.0 equimolar amount of DNA base pair, $[d(AT)_{10}]_2$ (Fig. 5C) and $[d(GC)_{10}]_2$ (Fig. 5D) gave different CD signals. These results strongly suggest that different binding-modes are used by **pPyNFP** to associate with $[d(AT)_{10}]_2$ and $[d(GC)_{10}]_2$. In the presence of dsDNA, the induced CD spectra were similar to those in the presence of $[d(GC)_{10}]_2$ (Fig. S3).

Effects of single-stranded DNA (ssDNA) were also examined using a 20-nucleotide oligomer (5'-TGTAGGCATGCTTAAGCAT-3'), which contains

approximately equal number of four nucleobases and thus, is unlikely to form particular secondary structures. In the presence of less than two equivalent molar amounts of nuleobase, a hypochromic change with a slight red-shift, in which *S-II* was shifted from 485 to 493 nm, was observed (Fig. 6A). In the presence of more than fourfold molar excess amounts of nucleobase, **pPyNFP** exhibited hyperchromic spectral change without a shift of λ_{max} (*S-II* was 495 nm) (Fig. 6B). This spectral change was closely similar to that seen in the presence of long dsDNA.

We finally addressed the importance of polymer structure of DNA by examining the effect of deoxyribonucleotide triphosphate (dNTP, equivalent mixture of dATP, dGTP, dCTP, and dTTP). Addition of dNTP caused modest hyperchromic change without red-shift (Fig. 7). This result suggests that dNTP modestly resolves aggregation of **pPyNFP**, but gives no significant electronic perturbation to the NFP macrocycle. Under the same conditions, **pPyP** only showed a very small spectral change upon addition of dNTP (Fig. S4).

Interactions of pPyNFP with G-quadruplex DNAs

G-quadruplex DNA structures, which are formed in the presence of K^+ or Na^+, have been considered to play pivotal roles on gene expression and DNA replication.[35-38] Because their biological importance makes G-quadruplex DNA structures attractive targets of DNA-binding ligands of small size[39-44] and some ligands have been subjected for *in vivo* anticancer studies.[45-47] We have examined the interactions between **pPyNFP** and G-quadruplex DNAs derived from human telomere sequence.

We first investigated the ability of **pPyNFP** to stabilize a K^+-induced G-quadruplex structure using the G4 DNA (5'-CATGGTGG-TTTGGG-$(TTAGGG)_3$-ACCAC-3') which has been used frequently for CD thermal melting experiments.[48,49] In the presence of K^+, G4 DNA exhibited a CD signal that is characteristic to a mixed (3+1) parallel/antiparallel structure[50] and is not influenced by **pPyNFP** (Fig. S5A). In the presence of 100 mM K^+ ions, melting temperature (T_m) of G4 DNA increased with increasing the concentration of **pPyNFP**, indicating that **pPyNFP** stabilizes a (3+1) parallel/antiparallel G-quadruplex structure (Table 1, see also Fig. S5B). Comparative measurement of CD melting curves with **pPyP** indicates that the extent of stabilization of the G-quadruplex structure by **pPyNFP** was nearly same to that by **pPyP** (Table 1, see also Fig. S5C).

Recently small size molecules with an ability to modulate G-quadruplex structures of the human telomeric sequence have been attracted considerable attention because they may be applicable to the regulation of telomerase activity.[51-56] The human telomeric sequence (5'-$(TTAGGG)_4$-3' abbreviated as $(T_2AG_3)_4$) adapts several types of G-quadruplex structures depending on the state of DNAs (in crystals or in solution) and monovalent metal ions (Scheme S1).[50,57-60] In solution, $(T_2AG_3)_4$ DNA forms a highly stable (3+1) parallel/antiparallel structure with K^+ (Scheme S1A),[50,57] and it also forms a (2+2) antiparallel structure with Na^+ (Scheme S1B).[58] The two types of G-quadruplexes exhibited different CD signals.[49] We investigated whether **pPyNFP** is capable of inducing structural change of G-quadruplex structures of $(T_2AG_3)_4$ DNA.

In the presence of K^+ ion which induces the highly stable (3+1)

parallel/antiparallel structure, the CD signal of $(T_2AG_3)_4$ DNA was unaffected by the addition of **pPyNFP** (Fig. 8A). This results is consistent with the observation that **pPyNFP** stabilizes K^+-induced G-quadruplex of G4 DNA (Fig. S5A). We then tested the (2+2) antiparallel structure induced by Na^+ (Fig. 8B). Upon the addition of **pPyNFP**, the characteristic CD signal of the (2+2) antiparallel structure (a positive peak around 245 nm and negative peak around 265 nm) was diminished and the CD signal showed a weak negative peak around 240 nm and a positive peak around 270 nm (Fig. 8B). The CD thermal melting profile showed that T_m of $(T_2AG_3)_4$ DNA structure with 100 mM Na^+ increased (+7.6 °C) upon addition of 5 molar equivalent of **pPyNFP** (Fig. S5D, Table S1), indicating that the DNA structure associated with **pPyNFP** was more stable than the initial (2+2) antiparallel structure induced by Na^+.

Since the CD spectra induced by **pPyNFP** was distinct from those induced by K^+ and Na^+, the resulting structure with **pPyNFP** may be different from the (3+1) parallel/antiparallel and (2+2) antiparallel structures. The CD spectra induced by **pPyNFP**, which exhibited a weak negative peak around 240–250 nm and a positive peak around 270 nm, share the features with the CD signals of parallel-type G-quadruplex structures that also exhibit a weak negative peak around 240 nm and a positive peak around 260–270 nm.[35,36] No similar change was observed upon addition of **pPyP** (Fig. S6). Although further analyses are needed, the CD analyses in this study suggest that **pPyNFP** interacts with $(T_2AG_3)_4$ DNA and can induce a parallel G-quadruplex structure in the absence of K^+. This possibility is also supported by the fact that $(T_2AG_3)_4$ DNA forms a parallel G-quadruplex structure in the single crystal

state (Scheme S1C). In the absence of monovalent metal ions, **pPyNFP** also induced a CD signal from DNA (Fig. S7A) which was similar to that in the presence of Na^+.

We are also interested in the influence of the stable (3+1) parallel/antiparallel DNA structure on the aggregation property of **pPyNFP**. In the absence of K^+ ions, the effect of G4 DNA on **pPyNFP** was closely similar to that observed with unstructured ssDNA (Fig. S7B). In the presence of 100 mM K^+ ions, however, the effects of $(T_2AG_3)_4$ DNA to **pPyNFP** were different from those of ss- and ds-DNAs. In the presence of less than 12 equimolar amounts of DNA bases (0.5 equimolar amounts of the G-quadruplex structure), hyperchromic effect was observed (Fig. 9A), suggesting that **pPyNFP** formed a sparsely aggregate. In the presence of more than 0.5 equimolar amounts of the G-quadruplex structure, a hypochromic spectral change was observed (Fig. 9B), suggesting that **pPyNFP** received electronic perturbation caused by π-π stacking interactions. Although determination of the accurate association constants (K_a's) of **pPyNFP** for $(T_2AG_3)_4$ DNA are difficult due to the complex spectral change (Fig. 9 and S8), we preliminarily estimated K_a's from the spectral change of **pPyNFP** with more than 12 equimolar amounts of DNA bases (Fig. 9B and Fig. S8B).[61] The roughly estimated K_a values are 5.6 X 10^6 M^{-1} and 1.7 X 10^7 M^{-1} in the presence of K^+ and Na^+ respectively. These values seem comparable to those of **pPyP** (2.4 X 10^7 M^{-1}) and **pPyNCP** (5.3 X 10^6 M^{-1}) for K^+-induced G-quadruplex formed by the human telomeric DNA sequence.[49]

In the presence of more than 12 equimolar amounts of DNA bases (0.5 equimolar amounts of the G-quadruplex structure), **pPyNFP** exhibited induced CD

signals (Fig. 9C) that were different from those induced by double stranded DNAs. These observations indicated that dose-dependent effects of the stable G-quadruplex DNA on **pPyNFP** were different from those of ss- and dsDNA.

Although the molecular mechanism causing such difference is not clear, higher order structures of G-quadruplex DNA might be involved in this spectral change.[60, 62-63] For instance, G-quadruplex DNAs could form an oligomeric structure, in which three G-quintets form a structural unit (G4 unit) and a TTA serves as a linker to connect two G4 units. Since the TTA linker region provides a molecular cleft (Scheme S2A), a possible model is that **pPyNFP** could be captured in the cleft between the G4 unit, in which NFP skeleton was sandwiched by two G-quintets flanked by the TTA linker. Alternatively, **pPyNFP** has an ability to assemble the monomeric G-quadruplex structure without oligomer formation (Scheme S2B).

Conclusions

We have synthesized a water-soluble derivative of N-fused porphyrin bearing cationic side-arms (**pPyNFP**) and elucidated its acid-base and DNA-binding properties. From pH-titration experiments, **pPyNFP** accepts two protons in a stepwise manner. UV-vis-NIR and induced-CD spectral changes upon additions of DNAs revealed that **pPyNFP** can bind to ss- and dsDNA. In the titration of **pPyNFP** with a long dsDNA, clear spectral changes were observed with 0.4 equimolar amounts of DNA base pairs. Under the same conditions, **pPyP** showed only a small spectral change with 0.5 equimolar amounts of DNA base pairs, suggesting that the binding affinity of **pPyNFP**

to dsDNA is even better than **pPyP**. This observation indicates that the NFP skeleton is a promising platform to develop high-affinity DNA binding molecules.

The induced CD spectra of DNA strongly suggest that **pPyNFP** can induce a structural change of $(T_2AG_3)_4$ DNA to an all-parallel structure. In contrast, such structural change was not induced by **pPyP**. Recently, it was also reported that **pPyNCP** induces a structural change of $(T_2AG_3)_4$ DNA to a (3+1) parallel/antiparallel structure. These observations indicate that the structural variation of tetrapyrrolic macrocycles (regular, N-fused, and N-confused porphyrins) gives distinct effects on $(T_2AG_3)_4$ DNA even though they possess the same pyridinium side-arms.

The present study also demonstrated that **pPyNFP** binds with G-quadruplex DNA with an affinity comparable to that between **pPyP** and G-quadruplex DNA. Since small size molecules recognizing higher order structures of G-quadruplexes are of significant interest,[63] comprehensive study on the interactions between oligomeric G-quadruplexes and water-soluble porphyrinoids is in progress. This study also implicates that the porphyrin-related macrocycles would be a promising toolbox for modulating the G-quadruplex DNAs and also their higher order structures. In addition, nucleophile-induced skeletal rearrangement of NFP to NCP has been reported.[22] As such skeletal conversion never achieved by regular porphyrins, it is attractive to apply this characteristic property to stimulus-induced regulation of G-quadruplex structures.

Experimental Section

Chemicals

For chemical synthesis, commercially available reagents and solvents were used without further purification. Silica gel column chromatography was performed on KANTO Silica Gel 60 N (spherical, neutral, particle size 40–50 μm). For preparation of aqueous buffer solutions for optical measurements, molecular biology grade reagents (Nacalai Tesque, Kyoto, Japan) and ultrapure water (prepared by Organo Puric-Z, Tokyo, Japan) were employed. Double stranded DNA (dsDNA) from salmon testes was purchased from Sigma-Aldrich Japan (Tokyo, Japan). Synthetic DNAs, which are ssDNA (5'-TGTAGGCATGCTTAAGCAT-3'), $d(AT)_{10}$ (5'-ATATATATATATATATATAT-3'), and $d(GC)_{10}$ (5'-GCGCGCGCGCGCGCGCGCGC-3'), were purchased from Hokkaido System Science (Hokkaido, Japan). G4 DNA (5'-CATGGTGG-TTTGGG-$(TTAGGG)_3$-ACCAC-3') and $(T_2AG_3)_4$ DNA (5'-$(TTAGGG)_4$-3') were purchased from Sigma-Aldrich Japan (Tokyo, Japan). Concentrations of DNA solutions were calculated from the absorbance at 260 nm. In DNA titration experiments, the molar ratios between the compounds and DNA were adjusted using the molar concentrations of DNA base pairs for dsDNA, $[d(AT)_{10}]_2$, and $[d(GC)_{10}]_2$, or with those of nucleobases for ssDNA, G4 DNA, and $(T_2AG_3)_4$ DNA, respectively.

Spectral measurements

^{1}H NMR spectra were recorded on a JEOL JNM-AL300 spectrometer (operating 300.40 MHz for ^{1}H). Chemical shifts were expressed in parts per million from a residual portion of deuterated solvent, $CHCl_3$ (δ = 7.26), DMSO (δ = 2.50). UV-vis-NIR

spectra were measured using 10 mm quartz cells at ambient temperature and spectra were recorded on a Shimadzu UV-3150PC spectrometer. CD spectra were recorded on a JASCO J-720 spectropolarimeter equipped with a PTC-423 L temperature controller using a quartz cell with an optical path length of 2 mm in a reaction volume of 600 μL and an instrument scanning speed of 100 nm/min, a 0.5 nm pitch, and a 1 nm bandwidth, with a response time of 2 s, over a wavelength range of 220–350 nm. The scan of the buffer was subtracted from the average scan for each sample. CD spectra were collected in units of molar circular dichroism versus wavelength. The cell holding chamber was flushed with a constant stream of dry nitrogen gas to prevent the condensation of water on the cell exterior. All DNA samples were dissolved and diluted in suitable buffers containing appropriate concentrations of ions. DNA samples were annealed at 95–98 °C for 5 min and then allowed to cool for 2 h to the initial temperature at which the samples were kept at the beginning of the experiment. CD data represent three averaged scans taken over a temperature range from 20 to 95 °C. All CD spectra are baseline-corrected for signal contributions caused by the buffer. The CD melting profiles were recorded at 295 nm. The temperature ranged from 20 to 99 °C, and the heating rate was 1.0 °C/min. The melting temperature (T_m) was defined as the temperature of the mid-transition point.

Synthesis

5,10,15,20-Tetrakis(*p*-(methoxymethoxy)methyl)phenyl)-2-aza-21-carbaporphyrin (1)

To a solution of pyrrole (2.081 mL, 30.0 mmol) and 4-methoxymethoxymethyl benzaldehyde (5.406 g, 30.0 mmol) in CH_2Cl_2 (3.0 L) at room temperature, methanesulfonic acid (1.363 mL, 21 mmol) was added. The mixture was stirred at room temperature for 30 min. Then 2,3-dichloro-5,6-dicyano-*p*-benzoquinone (DDQ) (5.99 g, 26.4 mmol) was added. After 1 min, triethylamine (11.7 mL, 84.0 mmol) was added. The reaction mixture was separated by column chromatography on a silica gel with CH_2Cl_2 as eluent. The second dark yellow-green fraction gave NCP **1** (1534.5 mg, 1.576 mmol) in 21% yield. ^{1}H NMR ($CDCl_3$): δ –5.04 (s, 1H, inner CH), 3.54 (s, 3H, -OCH_3), 3.55 (s, 3H, -OCH_3), 3.57 (s, 6H, -OCH_3), 4.90–4.93 (m, 16H, -OCH_2OCH_2-), 7.73 (d, *J* = 6.3 Hz, 4H, Ph), 7.82 (d, *J* = 7.8 Hz, 2H, Ph), 7.83 (d, *J* = 7.8 Hz, 2H, Ph), 8.11–8.15 (m, 4H, Ph), 8.31 (d, *J* = 7.8 Hz, 2H, Ph), 8.35 (d, *J* = 7.8 Hz, 2H, Ph), 8.53–8.57 (m, 3H, β-pyrrole), 8.59 (d, *J* = 5.1 Hz, 1H, β-pyrrole), 8.73 (s, 1H, outer α-pyrrole), 8.91 (d, *J* = 5.1 Hz, 1H, β-pyrrole), 8.96 (d, *J* = 4.8 Hz, 2H, β-pyrrole); MS (MALDI): *m/z* 910.39; UV-vis-NIR (CH_2Cl_2, λ_{max}/nm): 440.0, 542.5, 584.0, 728.5.

N-Fused 5,10,15,20-tetrakis(*p*-(methoxymethoxy)methyl)phenyl)porphyrin (4)

To a CH_2Cl_2 solution of NCP **1** (2.0 g, 2.195 mmol), NBS (899.0 mg, 5.05 mmol) was added, and the resulting solution was stirred for 10 min. The reaction mixture was separated on a silica gel column with CH_2Cl_2. The second green fraction gave dibrominated NCP **2** (1.60 g, 1.50 mmol) in 68.2% yield**.** Then, a pyridine solution of **2** (1558 mg, 1.46 mmol) was stirred for 12 h at ambient temperature. After evaporation, the residues were separated by chromatography on a silica gel column with CH_2Cl_2 as

eluent. The third red fraction gave monobrominated NFP **3** (772.0 mg, 0.781) in 54% yield. As fourth fraction, NFP **4** (115mg, 0.127 mmol) was obtained in 8.7% yield. A pyridine solution of monobrominated NFP **3** (772 mg, 0.781 mmol) was refluxed for 12 h. After evaporation, the residue was separated by chromatography on a silica gel column with CH_2Cl_2 as eluent. The third red fraction recovered unreacted **3** (317mg, 0.318 mmol, 41%), and the fourth red fraction gave NFP **4** (34 mg, 0.037 mmol) in 4.8% yield. ^{1}H NMR ($CDCl_3$): δ 3.51–3.60 (m, 12H), 4.78–4.95 (m, 16H), 7.62 (d, 1H, J = 4.8 Hz), 7.65–7.78 (m, 7H), 7.85 (d, 1H, J = 4.8 Hz), 7.95–8.00 (m, 3H), 8.05–8.10 (m, 5H), 8.40 (d, 2H, J = 6.1 Hz), 8.61 (d, 1H, 5.4 Hz), 8.74 (d, 2H, J = 8.4 Hz), 9.11 (d, 1H, J = 4.8 Hz), 9.30 (s, 1H); MS (MALDI): *m/z* 908.38; UV-vis-NIR (CH_2Cl_2, λ_{max}/nm): 361.5, 500.0, 548.5, 650.5, 706.0, 860.0, 943.0.

N-Fused 5,10,15,20-tetrakis(*p*-(hydroxymethyl)phenyl)porphyrin (5)

A trifluoroacetic acid (TFA) (5 mL) solution of **4** (107 mg, 0.146 mmol) was stirred for few minutes. Then, H_2O (5 mL) was added and the solution was sealed with a glass cap and stirred for 3 days. The reaction mixture was washed with aq $NaHCO_3$ solution and the precipitated product was filtrated. The obtained solid was purified with chromatography over a silica gel column (THF : Hexane = 5 : 1) to afford **5** in 71% yield (75.8mg, 0.103 mmol). ^{1}H NMR (DMSO-d_6): δ 4.70–4.87 (m, 8H), 5.25–5.50 (m, 4H), 7.47 (d, 1H, J = 5.1 Hz), 7.60–7.75 (m, 6H), 7.89 (d, 2H, J = 7.8 Hz), 7.94 (d, 2H, J = 7.8 Hz), 7.95–8.01 (m, 4H), 8.12 (d, 1H, J = 4.8 Hz), 8.24 (d, 2H, J = 7.8 Hz), 8.50 (d, 1H, J = 4.8 Hz), 8.63 (s, 1H), 8.84 (d, 2H, J = 8.4 Hz), 9.29 (s, 1H), 9.56 (d, 1H, J =

5.4 Hz); MS (MALDI): *m/z* 732.82; UV-vis-NIR (DMSO, λ_{max}/nm): 367.0, 500.5 550.5, 649.5, 705.5, 864.5, 951.0.

N-Fused 5,10,15,20-tetrakis(α-pyridinio-*p*-tolyl)porphyrin tetratrifluoroacetate salt (pPyNFP • $4CF_3COO^-$**)**

To a pyridine (1.0 mL) solution of **5** (5 mg, 0.0068 mmol) was added a pyridine solution (0.5 mL) of methanesulfonyl chloride (10.6 μL, 0.136 mmol) to yield a tetramesylate derivative **6**, which was further converted to **pPyNFP** in the solution. The resulting solution was stirred for 3 h at room temperature. The reaction mixture was filtrated and washed with pyridine and dichloromethane. Crude **pPyNFP** tetramethanesulfonate salt was dissolved in ultra-pure water and purified by HPLC with CosmoSil 5C18-AR-II (4.6×250 mm) using a mixed solvent CH_3CN/H_2O containing 0.1% TFA. Gradient conditions for CH_3CN in 0.1% aq TFA were as follows: 0–50% in 30 min. Flow rate was 1 mL/min and the absorption at 550 nm was employed for detection of NFP moiety. The desired fraction was collected and lyophilized to afford tetratrifluoroacetate salt of the target compound **pPyNFP** as dark-red solid. ^{1}H NMR (DMSO-d_6): δ 6.11–6.28 (m, 8H), 7.61 (s, 1H), 7.77–8.01 (m, 8H), 8.03–8.12 (m, 4H), 8.19 (d, 3H, J = 7.8 Hz), 8.23–8.40 (m, 9H)**,** 8.55 (d, 2H, J = 8.1 Hz)**,** 8.64 (d, 1H, J = 4.8 Hz), 8.68–8.82 (m, 4H)**,** 9.02 (d, 2H, J = 8.1 Hz), 9.40 (t, 4H), 9.48 (d, 4H, J = 6.6 Hz), 9.64 (s, 1H), 9.76 (s, 1H); HRMS (ESI^+): *m/z*; found: 245.103, calcd for $C_{64}H_{52}N_8$ (MH^+)/4: 245.107; UV-vis-NIR (DMSO, λ_{max}/nm): 367.5, 502.5 550.5, 652.0, 708.0, 857.0, 942.0.

Acknowledgments

We acknowledge Drs. Atsushi Maruyama and Naohiko Shimada for the help with measurements of CD spectra. This work is supported by Grants-in-Aids for Challenging Exploratory Research (No.23655159 to Y.I.), on Innovative Areas "Emergence in Chemistry" (No.21111518 to Y.I.) and "Emergence of highly elaborated π-space and its function" (No. 21108518 to H.F.), and also for the Global COE Program "Science for Future Molecular Systems" (H.F.) from the Ministry of Education, Culture, Sports, Science and Technology (MEXT), Japan.

References

1 K. M. Kadish, K. M. Smith and R. Guilard, *Handbook of Porphyrin Science*, World Scientific: Singapore, 2010, Vol. 1–15.

2 R. J. Fiel, J. C. Howard, E. H. Mark and N. Datta-Gupta, *Nucleic Acids Res.*, 1979, **6**, 3093–3118.

3 R. J. Fiel, J. *Biomol. Struct. Dyn.*, 1989, **6**, 1259–1274.

4 P. Kubát, K. Lang, P. Anzenbacher Jr., K. Jursíková, V. Král and B. Ehrenberg. *J. Chem. Soc., Perkin Trans. 1*, 2000, 933–941.

5 D. R. McMillin, A. H. Shelton, S. A. Bejune, P. E. Fanwick and R. K. Wall, *Coord. Chem. Rev.*, 2005, **249**, 1451–1459.

6 C. Romera, L. Sabater, A. Garofalo, I. M. Dixon and G. Pratviel, *Inorg. Chem.*, 2010, **49**, 8558–8567.

7 L. G. Marzilli, *New J. Chem.*, 1990, **14**, 409–420.

8 Y. H. Chae, B. Jin, J. K. Kim, S. W. Han, S. K. Kim and H. M. Lee, *Bull. Korean Chem. Soc*., 2007, **28**, 2203–2208.

9 J. Seenisamy, S. Bashyam, V. Gokhale, H. Vankayalapati, D. Sun, A. Siddiqui-Jain, N. Streiner, K. Shin-Ya, E. White, W. D. Wilson and L. H. Hurley, *J. Am. Chem. Soc*., 2005, **127**, 2944–2959.

10 Z. Gershman, I. Goldberg and Z. Gross, *Angew. Chem., Int. Ed*., 2007, **46**, 4320–4324.

11 A. K. Bordbar, M. Davari, E. Safaei and V. Mirkhani, *J. Porphyrins Phthalocyanines*, 2007, **11**, 139–147.

12 Y. Ikawa, S. Moriyama, H. Harada and H. Furuta, *Org. Biomol. Chem.*, 2008, **6**, 4157–4166.

13 X. Ragàs, D. Sánchez-García, R. Ruiz-González, T. Dai, M. Agut, M. R. Hamblin and S. Nonell, *J. Med. Chem.*, 2010, **53**, 7796–7803.

14 J. L. Sessler and S. J. Weghorn, *Expanded, Contracted & Isomeric Porphyrins*, Elsevier, Oxford, 1997.

15 P. J. Chmielewski and L. Latos-Grażyński, *Coord. Chem. Rev*., 2005, **249**, 2510–2533.

16 I. Gupta and M. Ravikanth, *Coord. Chem. Rev*., 2006, **250**, 468–518.

17 R. Misra and T. K. Chandrashekar, *Acc. Chem. Res*., 2008, **41**, 265–279.

18 Y. Inokuma and A. Osuka, *Dalton Trans.*, 2008, 2517–2526.

19 D. Sanchez-Garcia and J. L. Sessler, *Chem. Soc. Rev.*, 2008, **37**, 215–232.

20 J. Y. Shin, K. S. Kim, M. C. Yoon, J. M. Lim, Z. S. Yoon, A. Osuka and D. Kim, *Chem. Soc. Rev.*, 2010, **39**, 2751–2767.

21 H. Furuta, T. Ishizuka, A. Osuka and T. Ogawa, T. *J. Am. Chem. Soc.*, 1999, **121**, 2945–2946.

22 H. Furuta, T. Ishizuka, A. Osuka and T. Ogawa, *J. Am. Chem. Soc.*, 2000, **122**, 5748–5757.

23 T. Ishizuka, S. Ikeda, M. Toganoh, I. Yoshida, Y. Ishikawa, A. Osuka and H. Furuta, *Tetrahedron*, 2008, **64**, 4037–4050.

24 M. Toganoh, T. Kimura, H. Uno and H. Furuta, H. *Angew. Chem., Int. Ed*., 2008, **47**, 8913–8916.

25 Y. Ikawa, H. Harada, M. Toganoh and H. Furuta, *Bioorg. Med. Chem, Lett.*, 2009, **19**, 2448–2452.

26 S. Ikeda, M. Toganoh, S. Easwaramoorthi, J. M. Lim, D. Kim and H.Furuta, *J. Org. Chem.*, 2010, **75**, 8637–8649.

27 P. Hambright, in *The Porphyrin Handbook*, K.M. Kadish, K. M. Smith, and R. Guilard, Ed., Academic Press: California, 2000, Chapter 18.

28 S. Thyagarajan, T. Leiding, S. P. Arsköld, A. V. Cheprakov and S. A. Vinogradov, *Inorg. Chem.*, 2010, **49**, 9909–9920.

29 T. Weitner, A. Budimir, I. Kos, I. Batinić-Haberle and M. Biruš, *Dalton Trans.*, 2010, **39**, 11568–11576.

30 Y. Ikawa, H. Ogawa, H. Harada and H. Furuta, *Bioorg. Med. Chem. Lett.*, 2008, **18**, 6394–6397.

31 N. E. Mukundan, G. Petho, D. W. Dixon, M.-S. Kim and L. G. Marzilli, *Inorg. Chem.*, 1994, **33**, 4676–4687.

32 K. S. Dancil, L. F. Hilario, R. G. Khoury, K. U. Mai, C. K. Nguyen, K. S. Weddle and A. M. Shachter, *J. Heterocyclic. Chem.*, 1997, **34**, 749–755.

33 N. C. Maiti, M. Mazumdar and N. Periasamy, *J. Phys. Chem. B*, 1998, **102**, 1528–1538.

34 S. C. M. Gandini, I. E. Borissevitch, J. R. Perussi, H. Imasato and M. Tabak, *J. Lumin.*, 1998, **78**, 53–61.

35 J. R. Williamson, *Curr. Opn. Struct. Biol.*, 1993, **3**, 357–362.

36 S. Burge, G. N. Parkinson, P. Hazel, A. K. Todd and S. Neidle, *Nucleic Acids Res.*, 2006, **34**, 5402–5415.

37 H. J. Lipps and D. Rhodes, *Trends Cell. Biol.*, 2009, **19**, 414–422.

38 J. L. Huppert, *FEBS J.*, 2010, **277**, 3452–3458.

39 T. M. Ou, Y. J. Lu, J. H. Tan, Z. S. Huang, K. Y. Wong and L. Q. Gu, *ChemMedChem*, 2008, **3**, 690–713.

40 D. Monchaud, A. Granzhan, N. Saettel, A. Guédin, J. L. Mergny and M. P. Teulade-Fichou, *J. Nucleic Acids.*, 2010, pii 525862.

41 M. C. Nielsen and T. Ulven, *Curr. Med. Chem.*, 2010, **17**, 3438–3448.

42 S. Balasubramanian and S. Neidle, *Curr. Opin. Chem. Biol.*, 2009, **13**, 345–353.

43 Y. Xu, *Chem. Soc. Rev.*, 2011, **40**, 2719–27140.

44 D. J. Patel, A. T. Phan, and V. Kuryavyi, *Nucleic Acids Res.*, 2007, **35**, 7429–7455

45 A. M. Burger, F. Dai, C. M. Schultes, A. P. Reszka, M. J. Moore, J. A. Double, and S. Neidle, *Cancer Res.*, 2005, **65**, 1489–1496.

46 P. Phatak, J. C. Cookson, F. Dai, V. Smith, R. B. Gartenhaus, M. F. Stevens, and A. M. Burger, *Br. J. Cancer.*, 2007, **96**, 1223-1233.

47 T. Tauchi, K. Shin-ya, G. Sashida, M. Sumi, S. Okabe, J. H. Ohyashiki, and K. Ohyashiki, *Oncogene*, 2006, **25**, 5719–5725.

48 T. Yamashita, T. Uno and Y. Ishikawa, *Bioorg. Med. Chem*., 2005, **13**, 2423–2430.

49 Y. Du, D. Zhang, W. Chen, M. Zhang, Y. Zhou and X. Zhou, *Bioorg. Med. Chem.*, 2010, **18**, 1111–1116.

50 A. Ambrus, D. Chen, J. Dai, T. Bialis, R. A. Jones and D. Yang, *Nucleic Acids Res.*, 2006, **34**, 2723–2735.

51 K. Nakatani, S. Hagihara, S. Sando, S. Sakamoto, K. Yamaguchi, C. Maesawa and I. Saito, *J. Am. Chem. Soc.* 2003, **125**, 662–666.

52 D. P. Gonçalves, R. Rodriguez, S. Balasubramanian and J. K. Sanders, *Chem. Commun.*, 2006, 4685–4687.

53 D. P. Gonçalves, S. Ladame, S. Balasubramanian and J. K. Sanders, *Org. Biomol. Chem.*, 2006, **4**, 3337–3342.

54 B. Fu, J. Huang, L. Ren, X. Weng, Y. Zhou, Y. Du, X. Wu, X. Zhou and G. Yang, *Chem. Commun.*, 2007, 3264–3266.

55 S. Yang, J. Xiang, Q. Yang, Q. Zhou, X. Zhang, Q. Li, Y. Tang and G. Xu, *Fitoterapia*, 2010, **81**, 1026–1032.

56 S. K. Pradhan, D. Dasgupta and G. Basu, *Biochem. Biophys. Res. Comm.*, 2011, **404**, 139–142.

57 Y. Xu, Y. Noguchi and H. Sugiyama, *Bioorg. Med. Chem.*, 2006, **14**, 5584–5591.

58 Y. Wang and D. J. Patel, *Structure*, 1993, **15**, 263–282.

59 G. N. Parkinson, M. P. Lee and S. Neidle, *Nature*, 2002, **417**, 876–880.

60 D. Sen and W. Gilbert, *Biochemistry*, 1992, **31**, 65–70.

61 H. Mita, T. Ohyama, Y. Tanaka and Y. Yamamoto, *Biochemistry*, 2006, **45**, 6765–6772.

62 H.-Q. Yu, D. Miyoshi and N. Sugimoto, *J. Am. Chem. Soc.*, 2006, **128**, 15461–15468.

63 K. Shinohara, Y. Sannohe, S. Kaieda, K. Tanaka, H. Osuga, H. Tahara, Y. Xu, T. Kawase, T. Bando and H. Sugiyama, *J. Am. Chem. Soc.*, 2010, **132**, 3778–3782.

Legends

Chart 1

Structures of cationic water-soluble *meso*-tetraaryl porphyrins possessing four pyridinium moieties.

Chart 2

Basic structures of porphyrin (left), N-fused porphyrin (middle), and N-confused porphyrin (right).

Chart 3

Structure of **NFP-R9**, a water-soluble derivative of N-fused porphyrin possessing a nona-arginine (R9) peptide tail.

Scheme 1 Synthetic scheme of water-soluble cationic N-fused porphyrin (**pPyNFP**). Structures and chemical transformations of NCP derivatives and NFP derivatives in this study are summarized in top and bottom, respectively. Transformation of NCP (**2**) to NFP (**3**) is also shown. Reaction conditions: (i) NBS, 10 min, CH_2Cl_2; (ii) pyridine, rt, 12 h; (iii) pyridine, reflux, 12 h; (iv) TFA, H_2O, rt, 3 days; (v-a) methanesulfonyl chloride, pyridine; (v-b) pyridine, rt, 3h.

Scheme 2 A plausible aggregation/disaggregation behaviors of **pPyNFP** in the presence of different concentrations of SDS or DNA.

Fig. 1 UV-vis-NIR absorption spectra of **pPyNFP** and **NFTPP** in DMF.

Fig. 2 UV-vis-NIR absorption spectral changes of **pPyNFP** (7.5 μM) in H_2O titrated with NaOH and HCl. Absorption spectra for titration at pH 8.35–5.00 (A) and pH 2.20–0.58 (B).

Fig. 3 UV-vis-NIR absorption spectral changes of **pPyNFP** (7.5 μM) by the addition of various amounts of SDS at pH 8.5 (A), 7.0 (B), and 5.0 (C).

Fig. 4 Double stranded DNA (dsDNA) binding ability of **pPyNFP**.

A, B: UV-vis-NIR absorption spectra of **pPyNFP** (7.5 μM) in the presence of less (A) or more (B) than 1 equivalent molar amounts of dsDNA base pair at pH 7.0 with 50 mM HEPES.

C: Circular dichroism (CD) spectra of dsDNA in the absence and presence of **pPyNFP** at pH 7.0 with 50 mM HEPES.

Fig. 5 Interactions of **pPyNFP** with A:T and G:C base pairs.

A, B: UV-vis-NIR absorption spectra of **pPyNFP** (7.5 μM) in the presence of A:T (A) or G:C (B) base pairs at pH 7.0 with 50 mM HEPES.

C, D: Circular dichroism (CD) spectra of **pPyNFP** (7.5 μM) in the presence of A:T (C) or G:C (D) base pairs at pH 7.0 with 50 mM HEPES.

Fig. 6 Single stranded DNA (ssDNA) binding ability of **pPyNFP**.

UV-vis-NIR absorption spectra of **pPyNFP** (7.5 μM) in the presence of less (A) or more (B) than 1 equivalent molar amounts of ssDNA base at pH 7.0 with 50 mM HEPES.

Fig. 7 Effects of deoxyribonucleotide triphosphate on **pPyNFP**.

UV-vis-NIR absorption spectra of **pPyNFP** (7.5 μM) in the presence of deoxyribonucleotide triphosphate (dNTP) at pH 7.0 with 50 mM HEPES.

Fig. 8 Effects of **pPyNFP** onto different G-quadruplex DNA structures.

A: CD titration of $(T_2AG_3)_4$ DNA with the (3+1) parallel/antiparallel structure induced by 100 mM K^+ ions with 10 mM Tris-HCl (pH 7.4) and 1 mM EDTA.

B: CD titration of $(T_2AG_3)_4$ DNA with the (2+2) antiparallel structure induced by 100 mM Na^+ ions with 10 mM Tris-HCl (pH 7.4) and 1 mM EDTA.

Fig. 9 Effects of the stable G-quadruplex DNA structure on the absorption property of **pPyNFP**.

A, B: UV-vis-NIR absorption spectra of **pPyNFP** (7.5 μM) in the presence of less (A) or more (B) than 0.5 equivalent molar amount of the stable (3+1) parallel/antiparallel structure induced by 100 mM K^+ ions with 10 mM Tris-HCl (pH 7.4) and 1 mM EDTA.

C: Circular dichroism (CD) spectra of **pPyNFP** (7.5 μM) in the presence of the stable (3+1) parallel/antiparallel structure induced by 100 mM K^+ ions with 10 mM Tris-HCl (pH 7.4) and 1 mM EDTA.

Table 1. CD melting temperatures of G4 DNA in the presence of different concentrations of **pPyNFP** and **pPyP**.

Compound		*r* = [compound]/[G4 DNA]			
		0 (DNA alone)	1	3	5
pPyNFP	T_m (°C)	51.7 ± 0.6	54.3 ± 0.4	58.0 ± 0.4	60.7 ± 0.5
	ΔT_m (°C)	–	2.6 ± 0.2	6.3 ± 0.2	9.0 ± 0.1
pPyP	T_m (°C)	51.7 ± 0.6	55.6 ± 0.8	58.5± 0.4	61.1 ± 0.3
	ΔT_m (°C)	–	3.9 ± 0.2	6.8 ± 0.2	9.4 ± 0.4

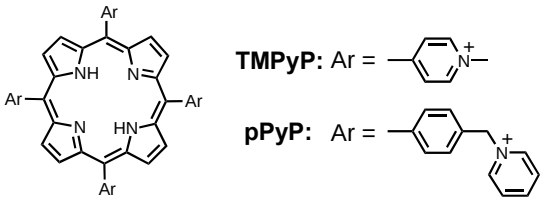

Chart 1

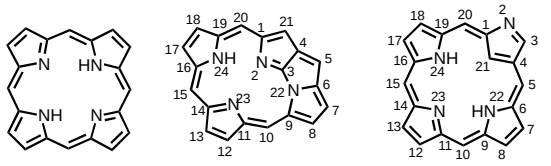

Chart 2

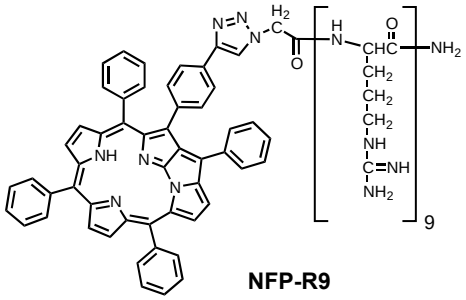

Chart 3

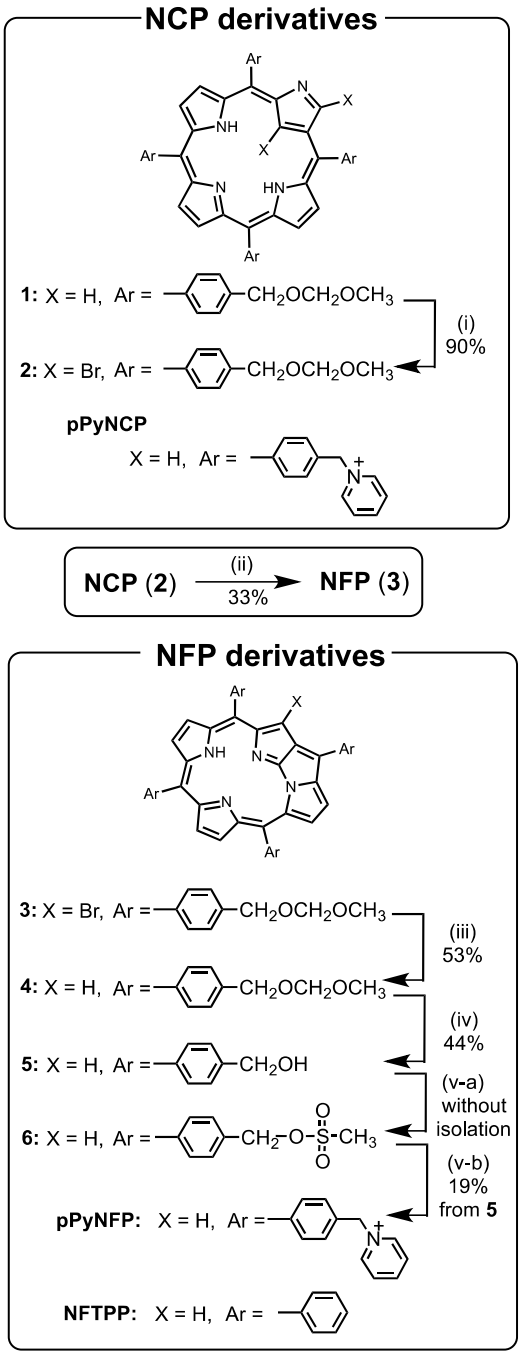
NCP derivatives
1: X = H, Ar = CH2OCH2OCH3
2: X = Br, Ar = CH2OCH2OCH3
(i)
90%
pPyNCP
X = H, Ar =
NCP (2)
(ii)
33%
NFP (3)
NFP derivatives
3: X = Br, Ar = CH2OCH2OCH3
4: X = H, Ar = CH2OCH2OCH3
5: X = H, Ar = CH2OH
6: X = H, Ar = CH2-O-S-CH3
(iii)
53%
(iv)
44%
(v-a)
without
isolation
(v-b)
19%
from 5
pPyNFP: X = H, Ar =
NFTPP: X = H, Ar =

Scheme 1

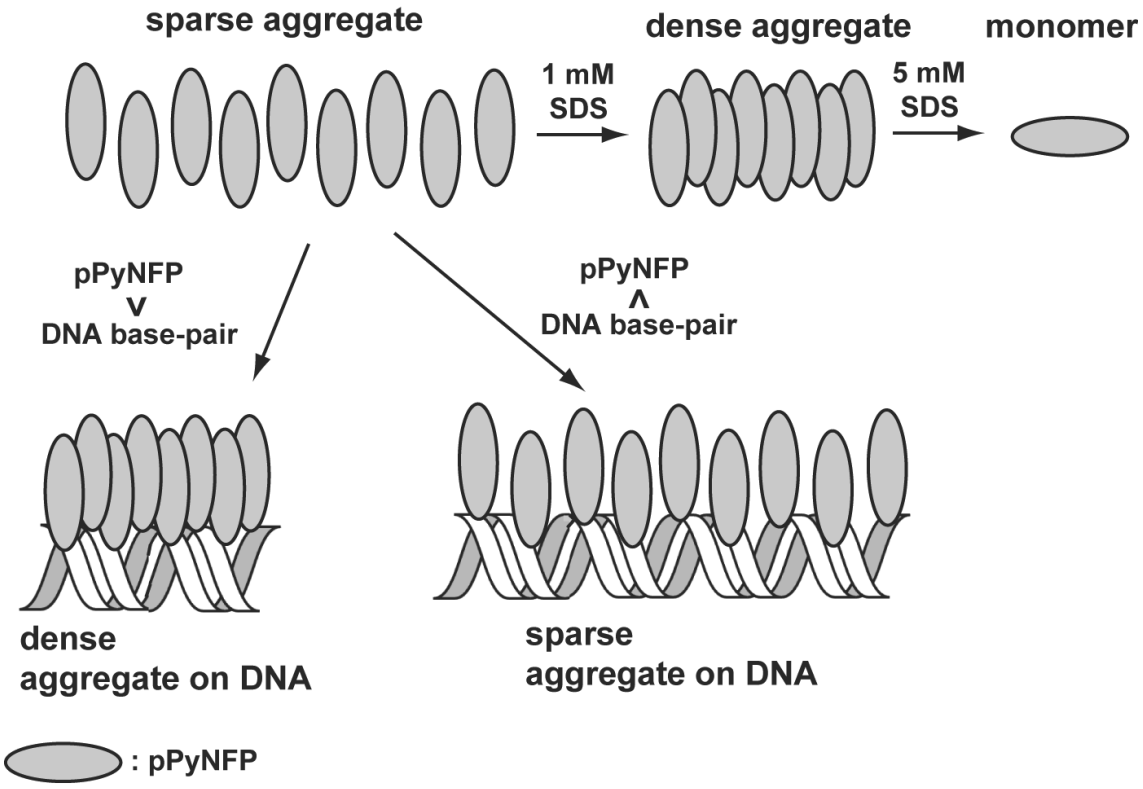
sparse aggregate
dense aggregate
monomer
1 mM
SDS
5 mM
SDS
pPyNFP
v
DNA base-pair
pPyNFP
^
DNA base-pair
dense
aggregate on DNA
sparse
aggregate on DNA
: pPyNFP

Scheme 2

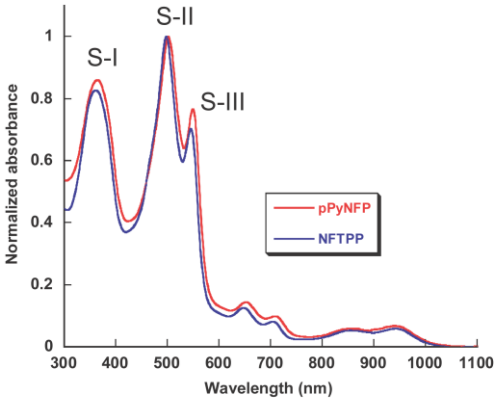

Fig. 1
(width 65 mm)

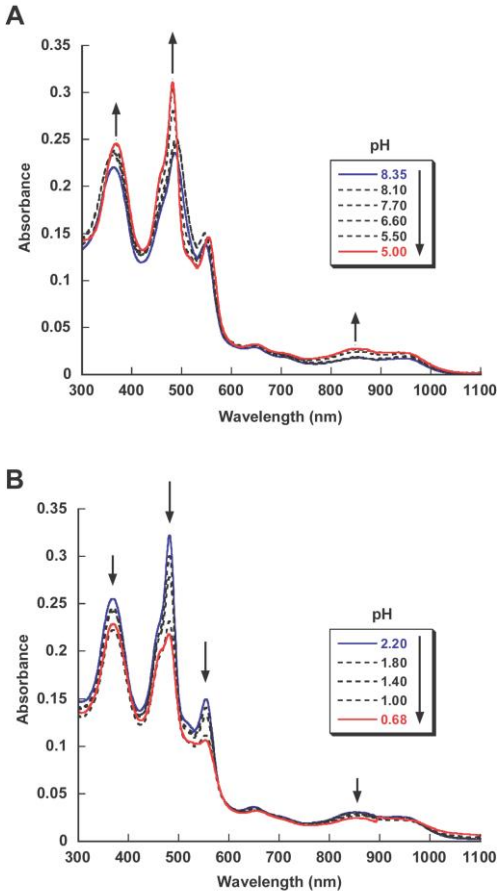

Fig. 2
(width 65 mm)

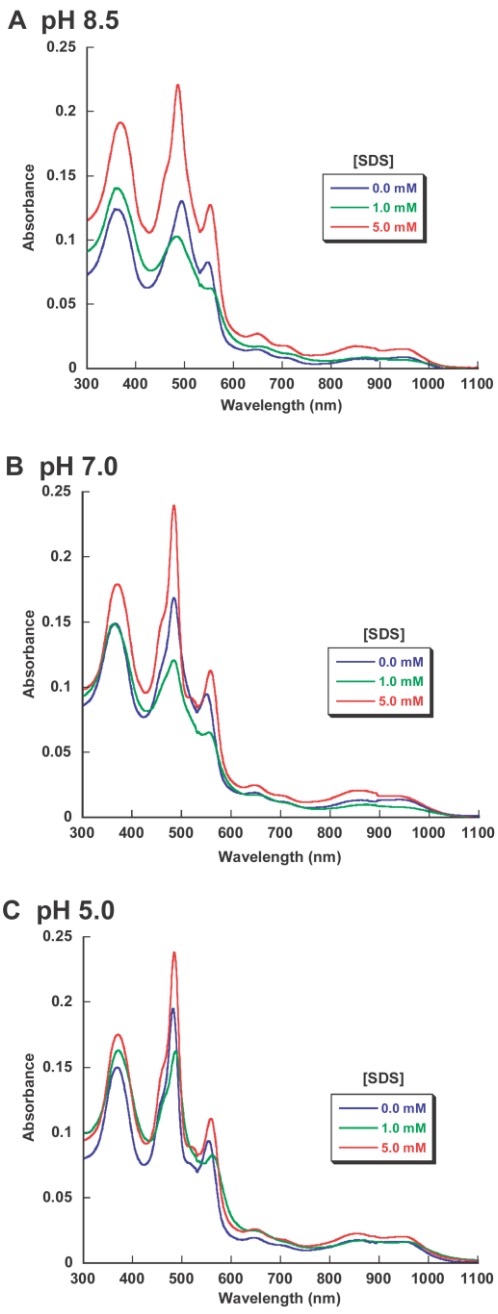

Fig. 3
(width 65 mm)

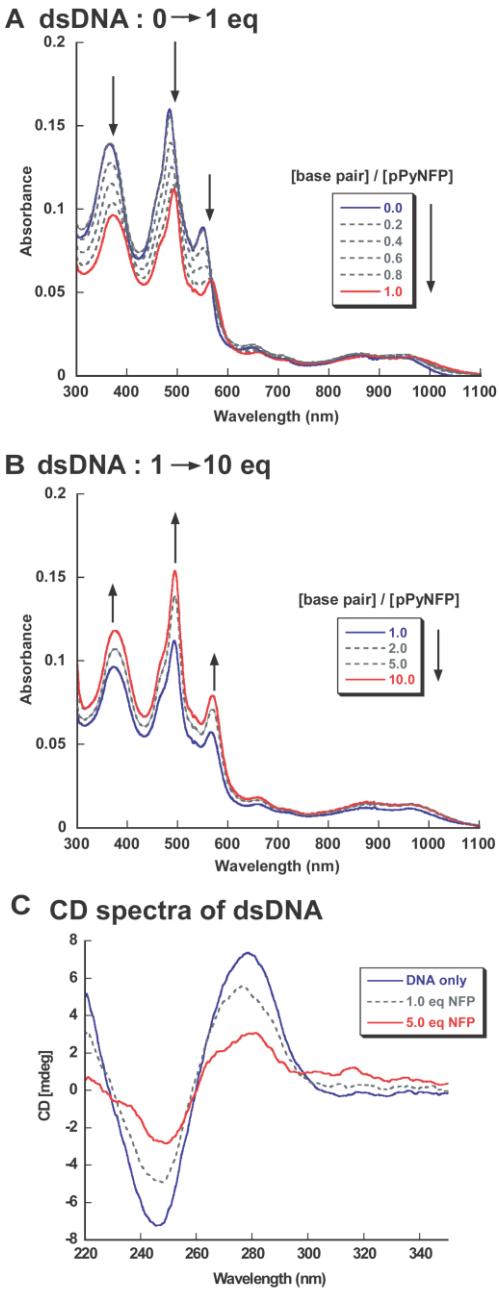

Fig. 4
(width 65 mm)

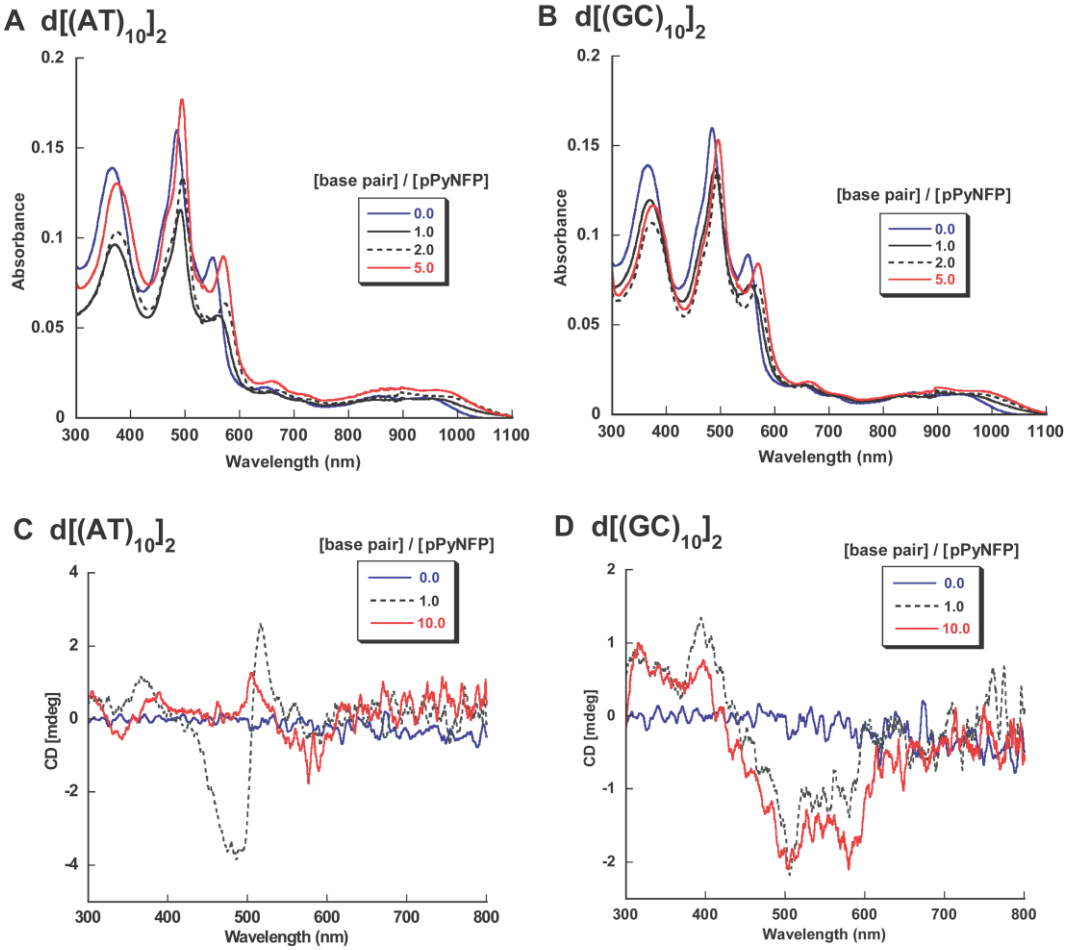

Fig. 5
(width 140 mm)

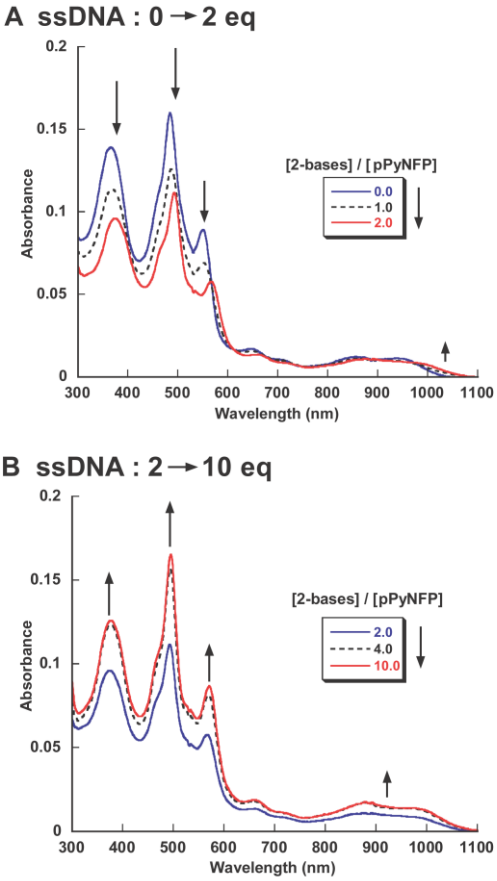

Fig. 6
(width 65 mm)

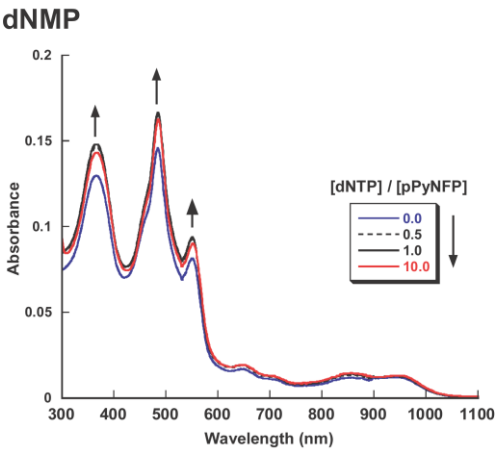

Fig. 7
(width 65 mm)

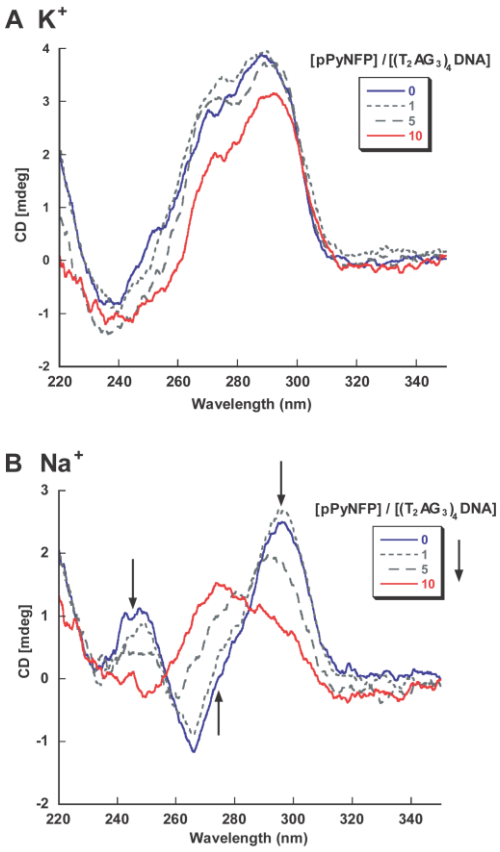

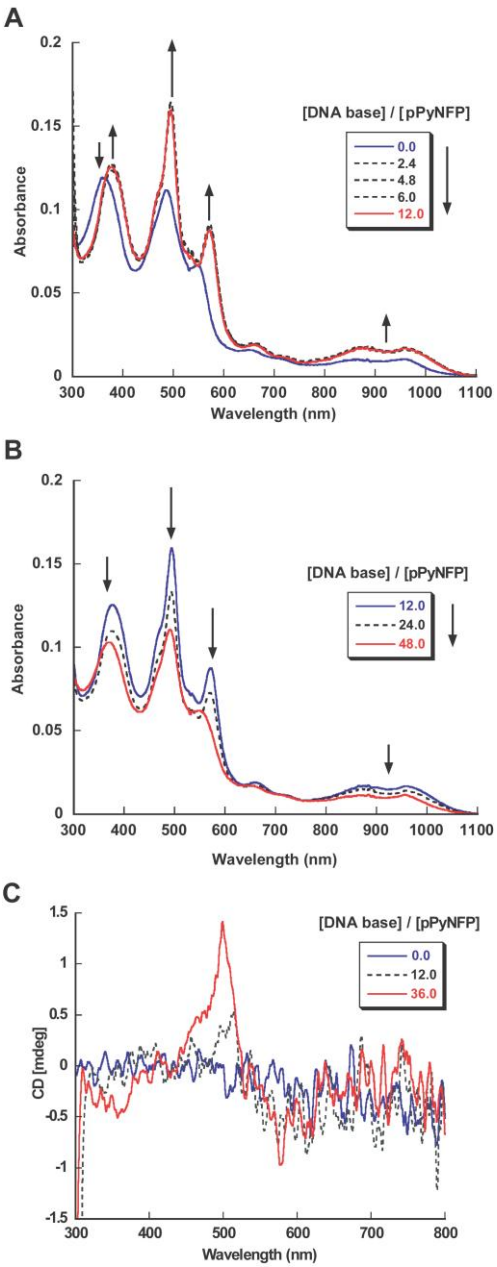

Fig. 8
(width 65 mm)

Fig. 9
(width 65 mm)

Table of Contents Entry Graphic